*sustainability*

MDPI

*Article*

# Waste-Derived Green Nanocatalyst for Biodiesel Production: Kinetic-Mechanism Deduction and Optimization Studies

**Chee Yoong Chooi [1], Jia Huey Sim [1,2,*], Shiau Foon Tee [1] and Zhi Hua Lee [1,2]**

[1] Department of Chemical Engineering, Lee Kong Chian Faculty of Engineering and Science, Universiti Tunku Abdul Rahman, Jalan Sungai Long, Bandar Sungai Long, Kajang 43000, Malaysia; knychooi@1utar.my (C.Y.C.); teesf@utar.edu.my (S.F.T.); leezh@utar.edu.my (Z.H.L.)

[2] Centre for Photonics and Advanced Materials Research (CPAMR), Universiti Tunku Abdul Rahman, Jalan Sungai Long, Bandar Sungai Long, Kajang 43000, Malaysia

* Correspondence: simjh@utar.edu.my or sjiahuey@gmail.com

**Abstract:** This research focuses on deducing the kinetic mechanism for biodiesel production catalyzed by a CaO nanocatalyst derived from waste cockle shells via thermal hydration–dehydration treatment. In addition, the CaO nanocatalyst preparation method via thermal hydration–dehydration-related parameters (hydration duration, recalcination temperature, and recalcination duration) was studied and optimized. The transesterification reaction catalyzed by the CaO nanocatalyst followed the Langmuir–Hinshelwood kinetic mechanism with surface reaction as the rate-limiting step. The relatively low activation energy (3786.7 J/mol) for a transesterification reaction offered by the CaO nanocatalyst enhanced the reaction rate to 27.3% FAME yield/hr. The optimal conditions for the thermal hydration–dehydration treatment used to develop the nano CaO catalyst were 6 h of hydration duration, 650 °C of recalcination temperature, and 3 h of recalcination duration. Of biodiesel yield, 94.13% was obtained at a moderate temperature of 60 °C and 3 h reaction time during the transesterification of palm oil catalyzed by the nano-CaO. SEM, BET, and TPD results proved that the CaO nanocatalyst had a large surface area (13.9113 $m^2/g$) and high pore volume (0.0318 $cm^3/g$) that were rich in active sites (1046.46 μmol $CO_2/g$), and the pore diameter (33.17 nm) was accessible to reactants and products.

**Keywords:** transesterification; biodiesel; nanocatalyst; fatty acid methyl ester (FAME); kinetic mechanism; rate law

check for updates

**Citation:** Chooi, C.Y.; Sim, J.H.; Tee, S.F.; Lee, Z.H. Waste-Derived Green Nanocatalyst for Biodiesel Production: Kinetic-Mechanism Deduction and Optimization Studies. *Sustainability* **2021**, *13*, 5849. https://doi.org/10.3390/su13115849

Academic Editor: Yusuf G. Adewuyi

Received: 8 April 2021
Accepted: 4 May 2021
Published: 22 May 2021

**Publisher's Note:** MDPI stays neutral with regard to jurisdictional claims in published maps and institutional affiliations.

**Copyright:** © 2021 by the authors. Licensee MDPI, Basel, Switzerland. This article is an open access article distributed under the terms and conditions of the Creative Commons Attribution (CC BY) license (https://creativecommons.org/licenses/by/4.0/).

## 1. Introduction

The rapid growth of the human population and industrialization has caused the fast diminishment of energy resources. The total global energy consumption is gradually increasing, and it marked at around 14,000 million tons of oil equivalent (MTOE) in 2019 [1]. Among fuel types, crude oil is still the main energy source, followed by natural gas and coal [1]. In order to ensure a sustainable energy supply in the future, the search of promising renewable fuel is a must. Thus, renewable-energy resources were discovered such as nuclear energy, hydroelectricity, and wind energy [2–4] to replace fossil fuels, since renewable-energy resources originate from natural cycles that are infinite and never exhausted.

Among renewable-energy resources, biodiesel has massive potential to replace crude oil. Biodiesel is a sustainable renewable resource and environmentally friendly compound. Compared to fossil fuels, the utilization of biodiesel as fuel reduces emissions of carbon monoxide, unburned hydrocarbons, and net carbon dioxide emissions per life cycle by significant amounts of 47%, 45%, and 78%, respectively [5]. The utilization of biodiesel power by vehicles can offset carbon dioxide emissions, as carbon dioxide emitted from biodiesel is eventually consumed by plants for photosynthesis [4]. Therefore, the burning of biodiesel does not contribute to global warming. Air pollution and acid rain can also

be minimized to a certain extent because of the significant reduction of sulfur content in biofuel [6]. Biodiesel can be applied in conventional diesel engines with a simple modification [3]. In comparison, biodiesel gives higher lubricity and durability than conventional diesel fuel does due to the absence of sulfur [7].

Nevertheless, biodiesel still cannot substitute crude oil as a primary energy source due to the comparatively higher selling price. The high production cost of biodiesel is partly due to difficulties in developing cheap catalyst materials with excellent catalyst properties. There are three different kinds of catalysts that are utilized in the transesterification process: acid [8], base [9], and enzyme [10] catalysts. Base and acid catalysts are more common compared to the enzyme ones, as they require a long chemical reaction for completion, and the enzyme operation cost is high [2]. Some problems arise during the transesterification reaction catalyzed by homogeneous catalysts, though homogeneous catalysts have better catalytic performance than that of heterogeneous catalysts [11]. The recovery of homogeneous catalysts involves a series of work steps, such as the neutralization of acidic or basic catalysts, the generation of large amounts of wastewater, and biodiesel drying with high moisture content at the end of the separation process. As a result, the operation cost is high, and the total duration of biodiesel production is long; thus, homogeneous catalysts are not favorable [12,13]. On the other hand, the operation of transesterification reaction with heterogeneous catalysts is usually cheap, with a simpler separation process, and the catalysts are more environmental friendly [14].

Nonetheless, there are some disadvantages with heterogeneous catalysts, such as a slower reaction rate, difficulty in catalyst preparation, and operating conditions are more energy-intensive [15,16]. The literature review showed that a calcium oxide (CaO) catalyst derived from different waste resources, such as egg shells [17] and abalone shells [18], possesses good catalytic activity with a biodiesel yield ranging 80–90%. The catalytic behaviors of CaO (derived from the same precursor) in the transesterification reaction to produce biodiesel from different types of cooking oil feedstock were similar. The literature review showed that researchers had used CaO as catalyst to produce biodiesel from different oil feedstocks, such as waste cooking oil [19], soybean oil [20], and sunflower oil [21]. However, catalytic performance is considered low in terms of reaction time, as it required more than 6 h to achieve high biodiesel yield. This low catalytic activity is due to the lower basicity than that of pure CaO and the reduced surface area of waste-material-derived CaO catalysts. The reaction rate of biodiesel can be improved by developing nanosized CaO catalysts. Following previous studies of developing micron-sized calcium oxide catalysts from egg shells and abalone shells, the current study aimed to synthesize a calcium oxide nanocatalyst derived from waste cockle shells by using the simple method of hydrolysis reaction and heat treatment.

Nanoparticles can be synthesized through two different methods, either a top–down or a bottom–up approach [22]. The bottom–up approach needs the reaction or agglomeration of suitable starting molecules with or without structure-directing agents [23], such as the sol-gel method, template-directed, precipitation, and microemulsion. For the top–down approach, bulk material is broken down into smaller particles by mechanical grinding [24], thermal breakdown [25], or chemical breakdown [26]. In comparison, the bottom–up approach involves critical reaction conditions with expensive precursors and structure-directing agents [27]. The top–down approach was preferable for the development of a heterogeneous nanosized CaO catalyst since natural-resource-derived catalysts have minimal pollution impact compared to catalysts synthesized from chemical substances.

In this research, the nano CaO catalyst was prepared via thermal hydration–dehydration treatment on waste cockle shells, with only water and heat applied. Parameters related to catalyst preparation via the thermal hydration–dehydration treatment, such as hydration duration, recalcination temperature, and recalcination duration, were studied and optimized. Characterization studies of nano CaO catalysts were carried out by using X-ray diffraction analysis (XRD), scanning electron microscopy (SEM) and Brunauer–Emmett–Teller (BET). The catalytic activity, and physical and chemical properties of the nano CaO catalysts prepared via

thermal hydration and dehydration treatments were compared with those of CaO catalysts prepared via the calcination method and waste cockle shells. Lastly, a kinetic mechanism for the transesterification process that was catalyzed by nano CaO catalysts derived from waste cockle shells was developed and verified with kinetic data.

## 2. Materials and Methods

### *2.1. Materials*

Buruh brand palmitic cooking oil was used to represent palm oil as oil feedstock for the transesterification reaction, and it was purchased from a grocery shop located in Bandar Sungai Long, Malaysia. Methanol ($CH_3OH$) and hexane ($C_6H_{14}$) of analytical grade with 99% purity were procured from Merck, Malaysia Ltd. Methyl heptadecanoate of analytical grade with 99% purity was purchased from Sigma Aldrich, Malaysia Ltd. and used as internal standard for gas-chromatography (GC) analysis.

### *2.2. Catalyst Preparation*

#### 2.2.1. Catalyst Prepared via Calcination Method

Waste cockle shells were washed and then rinsed with tap water. Cleaned cockle shells were dried in an oven at 80 °C overnight to remove water content. Cockle shells were then crushed into small pieces. Crushed cockle shells were then calcined in the furnace at 900 °C for 3 h.

#### 2.2.2. Catalyst Prepared via Thermal Hydration and Dehydration Method

The first stage of the thermal hydration and dehydration treatment is similar as the catalyst preparation method mentioned in Section 2.2.1. After the thermal treatment, CaO powder underwent hydration with distilled water at 60 °C for 3 h. The precipitate was then filtered and dried in the oven overnight at 80 °C to remove remaining water content. The hydrated CaO was recalcined in the furnace at 650 °C for 2 h. After the dehydration stage, a fine white powder of the nano CaO catalyst was synthesized.

### *2.3. Parameter Effects*

The effects of important parameters related to thermal hydration and dehydration treatment such as hydration duration, recalcination temperature, and recalcination duration were studied and optimized with the one-factor-at-a-time method. The effect of hydration duration was first optimized with varied duration (3, 4, 5, and 6 h). The other parameters of recalcination temperature and recalcination duration were constant at 650 °C and 3 h, respectively. After the optimal hydration duration had been determined, recalcination temperature was varied at 650, 750, 850, and 950 °C, while recalcination duration was constant at 3 h. Lastly, the recalcination-duration effect was studied at various values of 2, 3, 4, and 5 h.

### *2.4. Transesterification Reaction*

The catalytic activity of the CaO catalyst in the transesterification reaction was evaluated on the basis of achieved biodiesel yield. The transesterification reaction was performed in a 250 mL round-bottomed flask equipped with a condenser. Approximately 150 mL of cooking oil was mixed with methanol at a 8:1 methanol-to-oil molar ratio, and the mixture was stirred at 350 rpm [18]. The reaction was operated at a temperature of 60 °C and catalyzed with a 3 wt % CaO catalyst [28,29]. The biodiesel sample was collected at every 1 h, with a total duration of 3 h [30]. The biodiesel sample was centrifuged to separate the biodiesel layer from the mixture solution. The transesterification reaction was as shown in Equation (1):

$$\text{Triglycerides} + 3\text{Methanol} \rightleftharpoons \text{FAME} + 3\text{Glycerol} \quad (1)$$

### 2.5. Gas-Chromatography Analysis for Biodiesel

The biodiesel was obtained in the form of fatty acid methyl esters (FAME) from the transesterification of cooking oil that catalyzed by the nano CaO catalyst. There are four types of FAMEs, namely, methyl linoleate, methyl oleate, methyl palmitate, and methyl stearate.

The concentration of the produced biodiesel was analyzed by using gas chromatography (Perkin-Elmer Clarus 500 GC). Gas chromatography was equipped with Nukol$^{TM}$ FUSED SILICA (with dimensions of 30 m × 0.53 mm × 0.5 μm) and connected to the flame-ionization detector. Oven temperature was specified at 220 °C with a ramping rate of 10 °C min$^{-1}$. Helium was selected as the carrier gas for analysis with a flowrate of 3 mL min$^{-1}$.

Then, 250 μL of the internal standard, methyl heptadecanoate, was added into 250 μL of diluted FAME mixture. Of the mixtures, 1 μL was then injected into GC for analysis. The objective of this step was to determine the peak location of the methyl esters. The retention time of the peak location for each of the methyl esters is tabulated in Table 1.

**Table 1.** Fatty acid methyl ester (FAME) types and their retention time.

| FAME Types | Molecular Weight (g/mol) | Retention Time (min) |
|---|---|---|
| Methyl heptadecanoate (IS) | 284.48 | 13.27 |
| Methyl linoleate | 294.47 | 15.88 |
| Methyl oleate | 296.49 | 15.02 |
| Methyl palmitate | 270.45 | 12.17 |
| Methyl stearate | 298.50 | 14.65 |

Then, 100 μL of the FAME sample from biodiesel production was mixed with 200 μL of the internal standard, methyl heptadecanoate, with a concentration of 10 g/L. Next, 1 μL of the mixture was injected into GC. The concentration of the respective methyl ester present in the sample was then calculated by comparing the ratio of the peak methyl ester area to the peak internal-standard area. Biodiesel yield was calculated on the basis of Equation (2).

$$\text{Yield} = \frac{\text{Total concentration of methyl esters in biodiesel sample}}{\text{Theoretical concentration of methyl ester produced}} \times 100\% \quad (2)$$

### 2.6. Catalysts Characterization

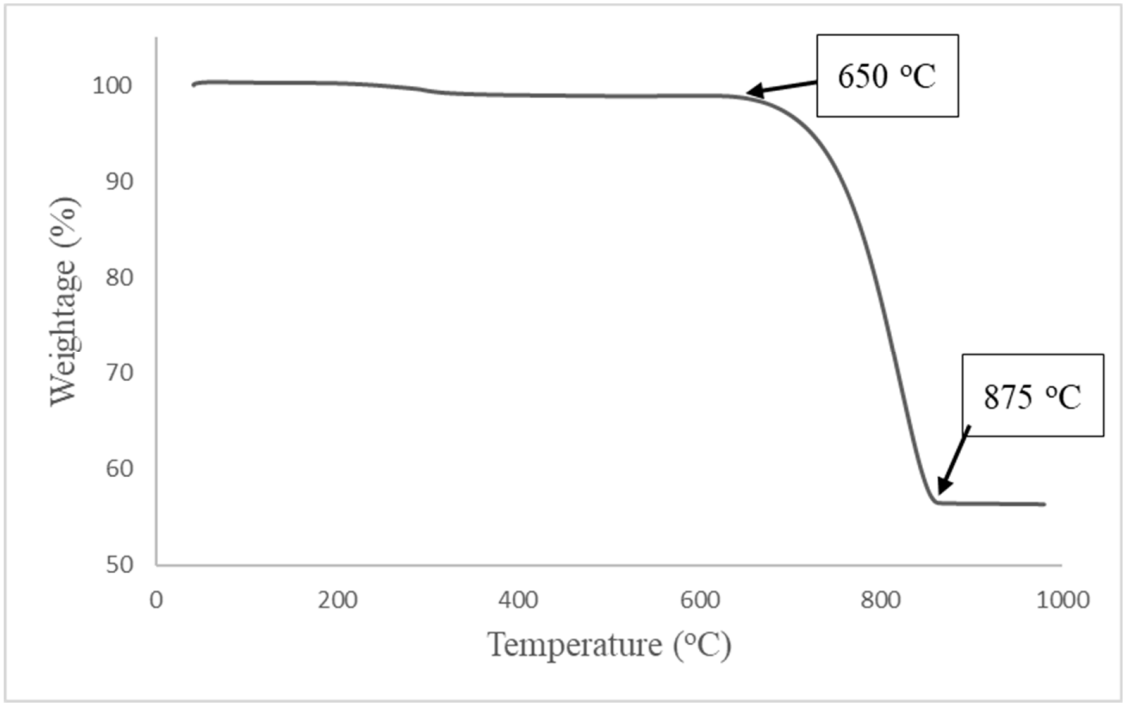
Numerous characterization studies were carried out to determine the physical and chemical properties of waste cockle shells, the CaO catalyst prepared via calcination method, the hydrated CaO, and the nano CaO catalyst prepared via thermal hydration–dehydration treatment. TGA characterization of the catalysts was performed by using Perkin Elmer STA 8000. Then, 15 mg of the catalyst sample was subjected to a heating rate of 20 °C min$^{-1}$ from 40 to 1000 °C under a flow of nitrogen gas. XRD of the catalyst was conducted through a Shimadzu X-ray diffractometer, XRD-6000 model. Cu–Kα radiation with 1.54 Å was used to create diffraction patterns at 40 kV. The catalyst sample was scanned with 2θ from 20° to 80° at a scanning rate of 2° min$^{-1}$. The surface morphology and elemental composition of the catalyst were analyzed by SEM coupled with an EDX instrument, Hitachi S-3400N model. For SEM analysis, the sample was coated with palladium and gold with an accelerating voltage of 15 kV. The basicity of the catalyst was analyzed via temperature-programmed desorption (TPD), Thermo Electron TPDRO 1100 model. Surface area, total pore volume, and pore diameter were analyzed by nitrogen physisorption. The equipment model used for nitrogen physisorption was Micromeritics 3 Flex Version 5.02.

## 3. Results

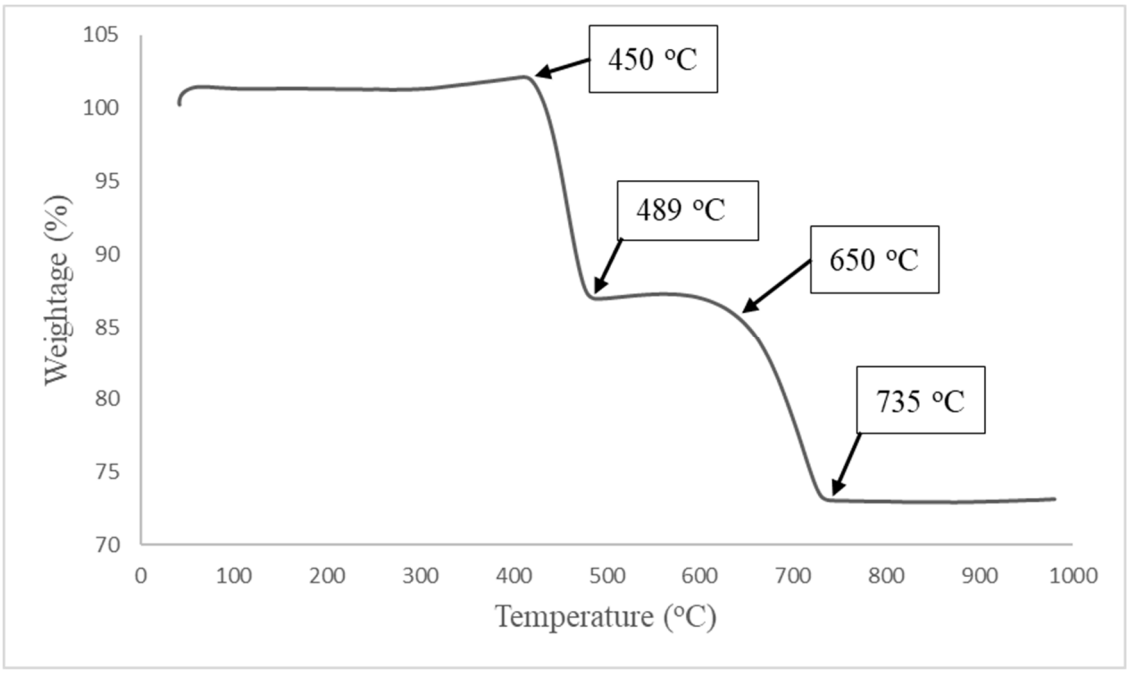
### *3.1. Catalyst-Characterization Results*

#### 3.1.1. Thermogravimetric (TGA) Analysis

Figure 1a shows the sudden declined weight of the waste cockle shells at 650 °C; the weight loss eventually reached a plateau at 875 °C. Figure 1a shows mass loss related to the release of carbon dioxide from the calcium carbonate compound due to thermal instability [31]. Figure 1b shows two decay steps of mass of hydrated CaO due to the heat decomposition of hydrated CaO [32].




(**a**)




(**b**)

**Figure 1.** Thermal decomposition of (**a**) waste cockle shells and (**b**) hydrated CaO.

The first mass-decay step occurred between 450 and 489 °C, and the second decay step was from 650 to 735 °C. The calcium hydroxide break in the calcium hydroxide–calcium oxide interphase was followed by the evolution of the water molecules during the first endothermic process. The decomposition of carbonaceous $CO_2$ materials from the catalyst occurred in the second endothermic process [33]. In summary, the complete transformation of $CaCO_3$ in the waste cockle shells into the active phase of CaO occurred at 875 °C. The desired recalcination temperature for the hydrated CaO sample was at 735 °C to achieve complete dehydration besides transforming the carbonaceous materials into the active CaO phase.

### 3.1.2. X-ray Diffraction (XRD) Analysis

X-ray diffraction was used to identify the phase, crystal structure, and average crystallite size of the CaO catalysts. The XRD diffraction patterns for the waste cockle shells, CaO catalyst prepared via calcination method, hydrated CaO and nano CaO catalyst prepared via thermal hydration–dehydration treatment are shown in Figure 2.

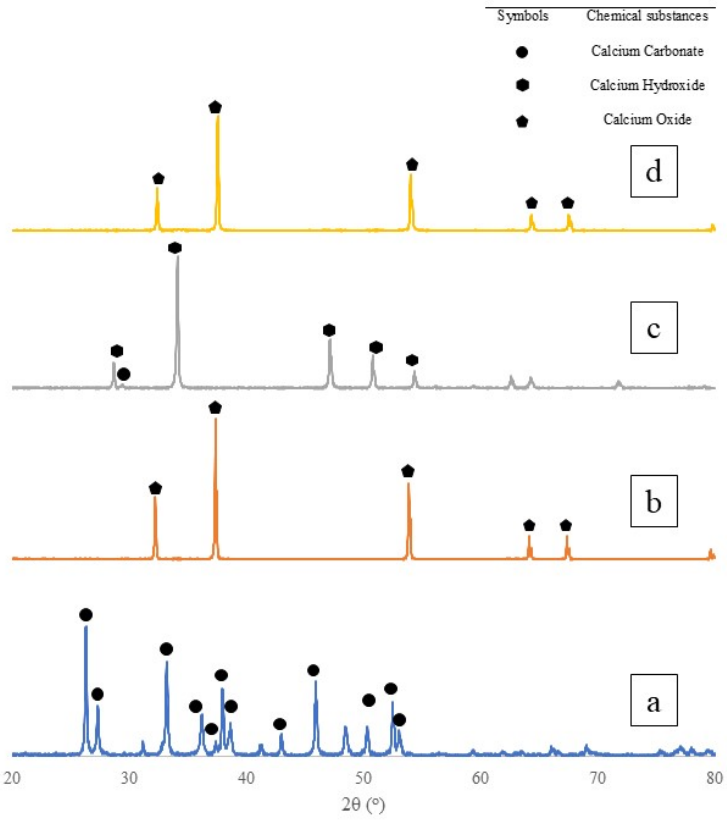



**Figure 2.** XRD diffraction pattern of (**a**) waste cockle shells, (**b**) CaO catalyst prepared via calcination method, (**c**) hydrated CaO, and (**d**) nano CaO catalyst prepared via thermal hydration–dehydration treatment.

The sharp peak formation indicated the formation of highly crystalline materials. In the diffraction pattern of the waste cockle shells, peaks with 2θ values of 26.2°, 27.2°, 33.1°, 36.2°, 37.9°, 38.4°, 42.9°,45.8°, 50.2°, 52.5°, and 52.9° could be indexed to basal planes (111), (021), (012), (200), (112), (130), (211), (220), (221), (132) and (113) diffraction for aragonite crystalline form of $CaCO_3$ [34] The peak of 2θ at 32.2°, 37.3°, 53.8°, 64.1°, and 67.3° could be indexed to the basal planes of (111), (200), (220), (311), and (222) [35] diffraction of CaO found in the CaO catalyst prepared via the calcination method and nano CaO catalyst prepared via thermal hydration–dehydration treatment [19]. This again indicated that the decomposition of calcium carbonate and calcium hydroxide in the nano CaO catalyst was accomplished during thermal hydration–dehydration treatment [36]. The

presence of calcium hydroxide peaks at 2θ values of 28.7°, 34.1°, 47.1°, 50.8°, 54.3°, 59.4°, 62.6°, and 71.8° with corresponding basal planes of (001), (101), (102), (110), (111), (021), (013), and (022) in hydrated CaO [37] is due to the reaction of calcium oxide with water during the hydration process [33].

#### 3.1.3. Scanning Electron Microscopy (SEM) Analysis

The morphologies of the raw cockle shells, CaO catalyst prepared via calcination method, hydrated CaO, and the nano CaO catalyst prepared via thermal hydration–dehydration treatment are shown in Figure 3. The surface of the raw cockle shells exhibited multiple layers of consistent rectangular shape with zero pore structures (Figure 3a). Figure 3b shows that the CaO catalyst derived from waste cockle shells via calcination at 900 °C presented a rough and porous structure with inconsistent small agglomerated particles. The formation of small particles with porous structures proved the formation of calcium oxide [38]. The formation of porous channels could be attributed to the release of carbon dioxide during the thermal-decomposition process [39].

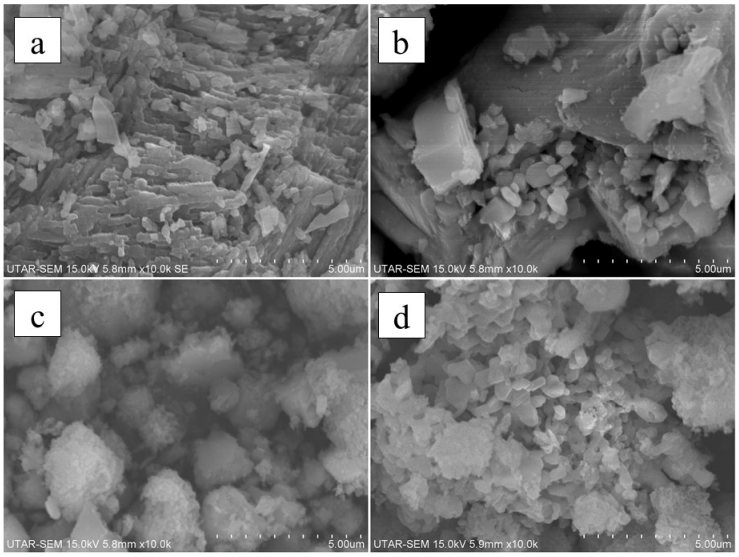



**Figure 3.** SEM characterization results for (**a**) waste cockle shells, (**b**) CaO catalyst prepared via calcination method, (**c**) hydrated CaO, and (**d**) nano CaO catalyst prepared via thermal hydration–dehydration treatment.

Figure 3c shows the hydrated CaO with a spherelike shape that had an uneven rough surface with low porosity. The porosities of the CaO catalyst prepared via the calcination method were reduced, and its particle size was increased due to the hydration reaction. When the CaO catalyst prepared via the calcination method was refluxed in water, there was a transformation of oxide structures into hydroxide structures, thereby increasing grain volume [40]. Figure 3d shows that the nano CaO catalyst prepared via thermal hydration–dehydration treatment had an appearance with highly porous and rough surface with a honeycomb shape and sharp edges [41]. This was due to the immediate shrinkage of the expanded hydroxide structures during calcination that caused the cracking on the surface of the nano CaO catalyst prepared via the thermal hydration–dehydration treatment [42]. The highly porous structures helped to increase the surface area of the nano CaO, which was beneficial for achieving a higher reaction rate.

Figure 4 shows the surface morphologies of the nano-CaO that was developed under different hydration durations. As the hydration hours were prolonged, the surface roughness and porosity of the nano CaO catalyst prepared by thermal hydration–dehydration treatment increased. The nano CaO catalyst pretreated with 6 h hydration duration presented nonuniform particle sizes and rough surfaces with a high number of sharp edges. The nano CaO under 3 h hydration treatment, on the other hand, presented rather smooth

surfaces and bulky particles with minimal pore structures. The prolonged hydration duration enhanced the formation of calcium hydroxide. The immediate water evaporation from the hydrated catalyst during calcination helped to increase the formation of irregular particle sizes with dense pores [40]. Thus, the catalytic properties of the nano CaO catalyst were enhanced by the thermal hydration–dehydration treatment.

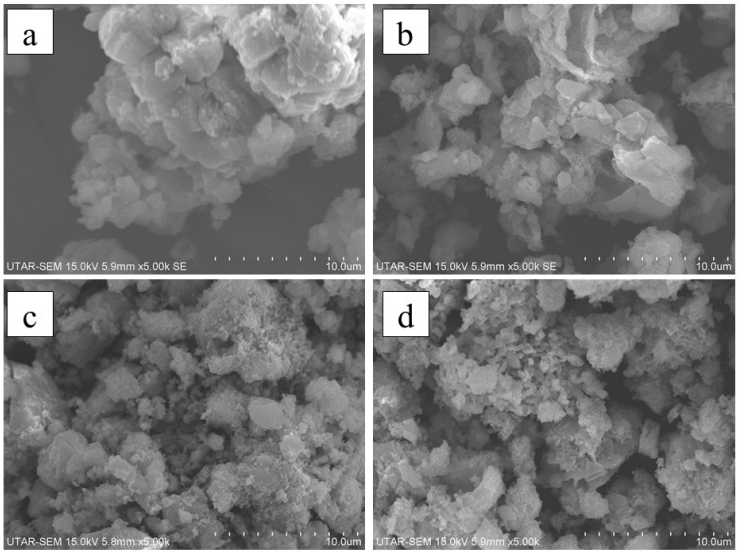



**Figure 4.** SEM characterization results for nano CaO at hydration duration of (**a**) 3 h, (**b**) 4 h, (**c**) 5 h, and (**d**) 6 h.

Figure 5 shows the surface morphologies of the nano CaO catalysts under different recalcination-temperature treatments. Nano CaO catalysts that developed under 950 °C recalcination temperature had the smoothest surface, while nano CaO catalysts recalcined at 650 °C had the roughest. As recalcination temperature increased, the sharp edges began to accumulate and stacked together, which further reduced the rough surface of the nano CaO catalysts, and the porous structures were demolished. This phenomenon was related to the sintering effects that commonly occur at high recalcination temperatures [43].

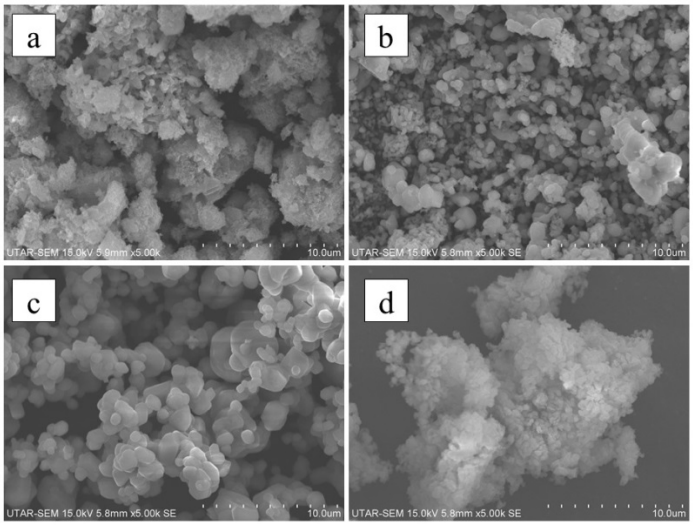



**Figure 5.** SEM characterization results for nano CaO at recalcination temperatures of (**a**) 650 °C, (**b**) 750 °C, (**c**) 850 °C, and (**d**) 950 °C.

Figure 6 shows the SEM images of nano CaO catalysts prepared under different recalcination durations. For nano CaO catalysts prepared under 2 h of recalcination,

the structures were low in porosity with less surface roughness. Compared to 3 h of recalcination, noticeable sharp edges and porous structures were observed. The sharp edges and pores on the surface of the nano CaO catalysts were gradually demolished once recalcination continued for longer than 3 h. This phenomenon is related to the sintering effects resulting from prolonged recalcination [33]. In summary, 6 h of hydration duration, 650 °C of recalcination temperature, and 3 h recalcination duration resulted in irregularly sized small particles with a high number of sharp edges and pores.

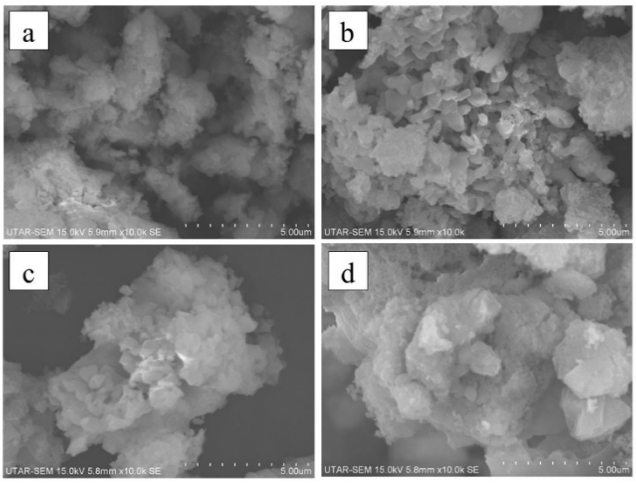



**Figure 6.** SEM characterization results for nano CaO at recalcination duration of (**a**) 2 h, (**b**) 3 h, (**c**) 4 h, and (**d**) 5 h.

### 3.1.4. Energy-Dispersive X-ray (EDX) Analysis

Table 2 shows the EDX results for four different samples. The elements that presented in the raw cockle shells were calcium, oxygen, and carbon.

**Table 2.** EDX results for samples.

| Samples | Average Weightage (wt %) | | |
|---|---|---|---|
| | C | O | Ca |
| Waste cockle shells | 12.48 | 44.64 | 41.20 |
| CaO catalyst prepared via calcination treatment | 0.00 | 16.72 | 83.28 |
| Hydrated CaO | 4.23 | 35.31 | 60.47 |
| Nano CaO prepared via thermal hydration–dehydration treatment | 2.29 | 16.06 | 75.65 |

For CaO catalysts prepared via the calcination method, hydrated CaO, and nano CaO catalysts prepared via thermal hydration–dehydration treatment, the major detected elements were calcium and oxygen, which indicated that the removal of carbon dioxide occurred during calcination treatment. Mild content of carbon and oxygen elements in CaO catalyst prepared via calcination method and nano CaO catalyst prepared via thermal hydration–dehydration treatment showed that the catalysts mostly occupied CaO active sites, reflecting its better catalytic activity. According to Rodriguez-Garcia et al. [44], the presence of carbon atoms in the catalyst was due to the contamination of the catalyst with $CO_2$ when the catalyst was exposed to the atmosphere.

### 3.1.5. Temperature-Programmed Desorption (TPD) Analysis

The basicity of catalysts indicated the number of available active sites in the catalyst during the chemical reaction. In order words, the catalyst with higher basicity had better catalytic performance compared to the catalyst with lower basicity [40]. The basicity of the CaO catalyst prepared via the calcination method and the nano CaO catalyst prepared

via thermal hydration–dehydration treatment was determined by using temperature-programmed desorption (TPD) analysis. Table 3 shows the total basicity of both catalysts.

**Table 3.** Total catalyst basicity.

| Catalyst | Total Basicity (μmol $CO_2$/g) |
|---|---|
| CaO prepared via calcination method | 464 |
| Nano CaO prepared via thermal hydration–dehydration treatment | 1046 |

Table 3 shows that the nano CaO catalyst had total recorded basicity of 1046 μmol $CO_2$/g, which was twice higher than the CaO catalyst's basicity (464 μmol $CO_2$/g). This proved that the number of active sites in the nano CaO catalyst was greater than that of the CaO catalyst. Thus, the catalytic performance of the nano CaO catalyst was successfully enhanced by the thermal hydration–dehydration treatment.

#### 3.1.6. Nitrogen Physisorption

The nitrogen physisorption results in Table 4 show that the thermal hydration–dehydration method enhanced the surface morphology of the CaO catalyst in terms of surface area and total pore volume.

**Table 4.** Nitrogen physisorption results of CaO catalyst prepared via calcination treatment and nano CaO catalyst prepared via thermal hydration–dehydration treatment.

| Sample | Multipoint BET ($m^2$/g) | Total Pore Volume ($cm^3$/g) | Average Pore Diameter (nm) | Biodiesel Yield at 3 h Reaction Time (%) |
|---|---|---|---|---|
| CaO catalyst prepared via calcination treatment | 0.710 ± 0.004 | 0.006 | 124 | 10 |
| Nano CaO catalyst prepared via thermal hydration–dehydration treatment | | | | |
| 650 °C recalcination temperature | 13.9 ± 0.2 | 0.032 | 33.2 | 94 |
| 950 °C recalcination temperature | 10.2 ± 0.08 | 0.022 | 41.8 | 49 |

The nano CaO catalyst (at 650 °C recalcination temperature) had higher surface area and total pore volume of 13.9 $m^2$ $g^{-1}$ and 0.032 $cm^3$ $g^{-1}$, respectively, compared to those of the CaO catalyst prepared via the calcination method, with 0.710 $m^2$ $g^{-1}$ and 0.006 $cm^3$ $g^{-1}$, respectively. The pore diameter of the CaO catalyst was mildly affected by the thermal hydration–dehydration treatment where the pore diameters of the CaO catalyst and nano CaO were 124 and 33.2 nm, respectively. The nano CaO catalyst that developed under a calcination temperature of 650 °C had higher surface area and pore volume than those of the calcination temperature of 950 °C. The sintering effect occurred in the structure of the nano CaO catalyst when the catalyst was developed under high recalcination temperatures of 950 °C and above. The sintering effect is the change in catalyst structures with small particles tending to chemically bind together to form large particles under heat treatment. The sintering effect always results in low BET surface area and low pores volumes [45]. During the sintering effect, active CaO sites tended to agglomerate and reduce the surface area of the nano CaO catalyst [46].

The average pore diameter of the nano CaO particles could affect the reaction rate of transesterification. According to Chang, H.J. and Crynes [47], a smaller pore diameter may cause product accumulation inside the pores, which can deactivate the active sites. In contrast, the rate of reaction may not be affected by a larger pore diameter due to the slow accumulation of products. Table 3 shows that the rate of reaction and biodiesel yield were not influenced by the smaller pore diameter of the nano CaO catalysts (33–41 nm) compared to the pore diameter of CaO catalyst (124 nm). Thus, the limiting factor of the smaller pore diameter in the nano CaO catalyst can be eliminated.

Triglycerides and methanol were the reactants for transesterification reaction. Four major types of fatty acids were found in palm oil, namely, palmitic acid, stearic acid, oleic

acid, and linoleic acid. According to Shuit et al. [48], palmitic acid has a spatial width of 0.37 nm, stearic acid of 0.25 nm, oleic acid of 0.72 nm, and linoleic acid of 1.13 nm. Methanol molecules have a kinetic diameter of around 0.39 nm [49]. For the products of the transesterification reaction, the molecular size of glycerol and biodiesel was 0.10 and 0.64 to 1.52 nm, respectively [50]. Thus, available active sites at the inner pores of the nano CaO catalyst, with an average pore diameter of 33–41 nm, were accessible to reactants and products with molecular sizes of 0.10–1.52 nm.

### *3.2. Optimization of Thermal Hydration–Dehydration Treatment*

#### 3.2.1. Effect of Hydration Duration

Figure 7 shows that the biodiesel yield increased with increased hydration duration. Biodiesel yield increased according to the following sequence of hydration duration: 4 h < 5 h < 6 h. The increasing trend of biodiesel yield with lengthy hydration duration was reported by Asikin-Mijan et al. [40],. During the hydration treatment on the CaO catalyst, a hydroxylation reaction occurred on the surface of CaO, which promoted the formation of hydroxides. The CaO catalyst with many hours of contact with water accelerated the growth of the $Ca(OH)_2$ layers. The heat decomposition of water molecules from the $Ca(OH)_2$ lattice structure during recalcination led to the fractionation of crystallites into smaller particle sizes, thus promoting high surface area, high porosity, and pore volume [51] The morphology of the catalysts was examined via SEM analysis, and the characterization results agreed with catalytic performance. Results proved that prolonged hydration duration enhanced the catalytic activity of the catalysts, thereby leading to high biodiesel yield. The 6 h duration was determined to be the optimal hydration duration in subsequent optimization studies.

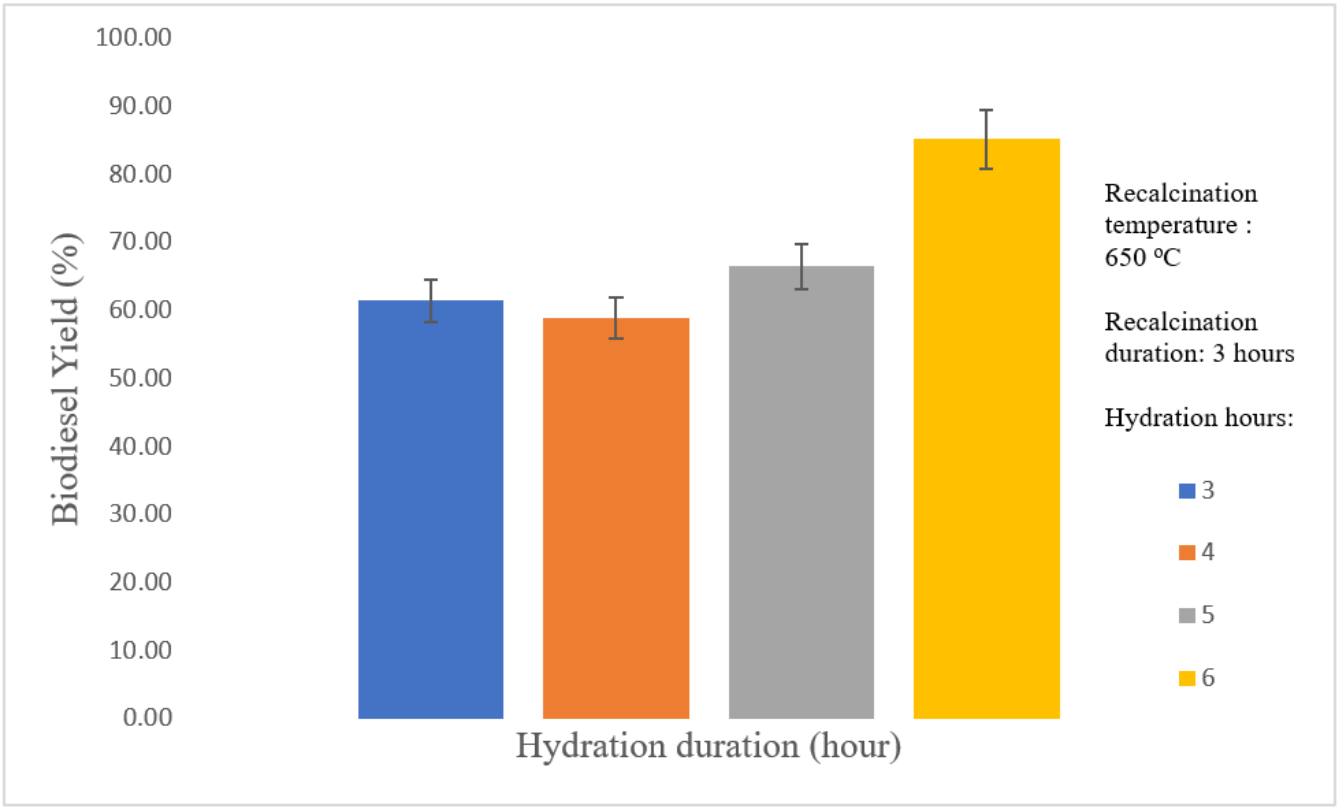



**Figure 7.** Effect of hydration duration on biodiesel yield.

### 3.2.2. Effect of Recalcination Temperature

Figure 8 shows that biodiesel yield was inversely proportional to recalcination temperature. For a 3 h reaction, the highest achieved biodiesel yield was 91.3% for the catalyst recalcined at temperature of 650 °C. The achieved biodiesel yield was reduced with increased recalcination temperature, where only 52.66% biodiesel yield was achieved for the catalyst recalcined at 950 °C. This occurrence can be linked to the sintering effects of the nano CaO catalyst when recalcined under high temperatures [43]. As calcination temperature increased, the rough structure of the nano CaO catalyst was gradually demolished due to the agglomeration of small particles. The morphology of the catalysts was discussed in SEM analysis, and the characterization results agreed with catalytic performance.

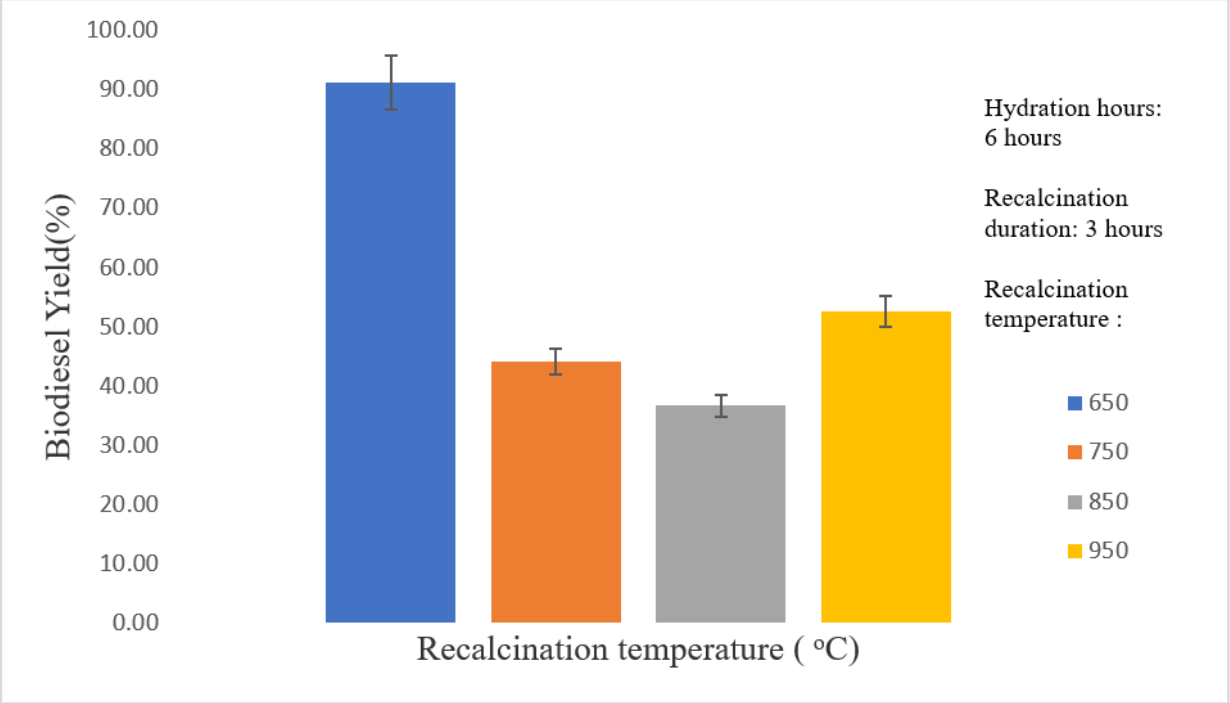



**Figure 8.** Effect of recalcination temperature on biodiesel yield.

According to Smith et al. [43], the highest biodiesel yield was obtained when the reaction had been catalyzed by the catalyst prepared under 650 °C calcination temperature. As the calcination temperature of the prepared catalyst gradually increased from 650 to 1100 °C, a decreasing trend of biodiesel yield was observed. In the current study, 650 °C was selected as the optimal recalcination temperature in subsequent optimization studies.

### 3.2.3. Effect of Recalcination Duration

Figure 9 shows that prolonged recalcination of more than 4 h can gradually reduce biodiesel yield. For the nanocatalyst recalcined for 3 h, the highest achieved biodiesel yield was 94.13% at 3 h reaction time, whereas the lowest biodiesel yield of 30.15% was achieved with the nanocatalyst recalcined for 5 h. This is because the sintering effects occurred in the nano CaO catalyst when the catalyst was recalcined for more than 4 h.

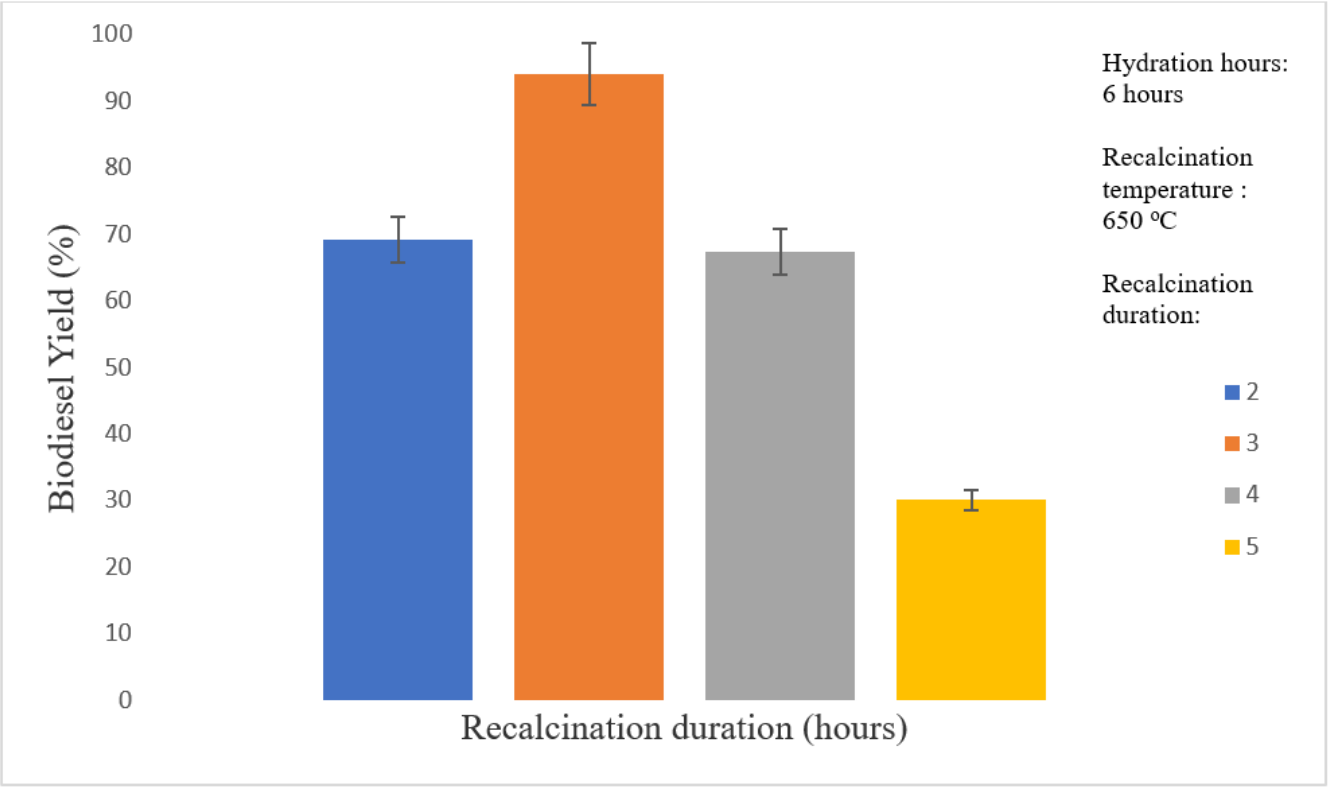



**Figure 9.** Effect of recalcination duration on biodiesel yield.

The small particles in the nano CaO catalyst started to agglomerate and form larger particles. This indirectly reduced the number of active sites and the specific surface area of the nano CaO catalyst prepared via thermal hydration–dehydration treatment [46]. The morphologies of the catalysts were discussed in SEM analysis, and characterization results agreed with catalytic performance. In the study, 3 h was selected as the optimal recalcination duration for nano CaO catalyst preparation via the thermal hydration–dehydration treatment.

### *3.3. Kinetic Mechanism*

A kinetic study was carried out on the transesterification reaction catalyzed by the nano catalyst derived from waste cockle shells. The kinetic mechanism of the nano CaO catalyst prepared via thermal hydration–dehydration treatment was deduced, followed by the development of kinetic model. Stoichiometrically, one unit of triglycerides (*TG*) reacted with three units of methanol (*M*) to obtain three moles of biodiesel (*FAME*) and one mole of glycerol (*G*). The reaction steps for biodiesel production are below:

Adsorption: $TG + S \rightleftharpoons TG.S$

$$r_a = k_a C_{TG} C_S - k_{-a} C_{TG.S} \quad (3)$$

where $r_a$ = reaction rate of adsorption; $k_a$ = rate constant of forward reaction; $k_{-a}$ = rate constant of backward reaction; $C_{TG}$ = concentration of triglycerides; and $C_S$ = number of vacant sites.

Given that $K_a = \frac{k_a}{k_{-a}}$, the ratio of the rate constant of the forward reaction to the rate constant of the backward reaction was

$$r_a = k_a (C_{TG} C_S - \frac{C_{TG.S}}{K_a}) \quad (4)$$

Surface reaction: $TG.S + M \rightleftharpoons FAME.S + G$

$$r_s = k_s C_{TG.S} C_M - k_{-s} C_{FAME.S} C_G \quad (5)$$

where $r_s$ = reaction rate of surface reaction; $k_s$ = rate constant of forward reaction; $k_{-s}$ = rate constant of backward reaction; $C_M$ = methanol concentration; $C_{TG \cdot S}$ = concentration of triglycerides attached to vacant sites; $C_{FAME.S}$ = concentration of FAME attached to vacant sites; and $C_G$ = glycerol concentration.

Given that $K_s = \frac{k_s}{k_{-s}}$, the ratio of the rate constant of the forward reaction to the rate constant of the backward reaction was

$$r_s = k_s (C_{TG.S} C_M - \frac{C_{FAME.S} C_G}{K_s}) \quad (6)$$

Desorption: $FAME.S \rightleftharpoons FAME + S$

$$r_d = k_d C_{FAME.S} - k_{-d} C_{FAME} C_S \quad (7)$$

where $r_d$ = reaction rate of desorption; $k_d$ = rate constant of forward reaction; and $k_{-d}$ = rate constant of backward reaction.

Given that $K_d = \frac{k_d}{k_{-d}}$, the ratio of the rate constant of the forward reaction to the rate constant of the backward reaction was

$$r_d = k_d (C_{FAME.S} - \frac{C_{FAME} C_s}{K_d}) \quad (8)$$

3.3.1. Derivation of Kinetic-Rate Equation

Some assumptions were made before the derivation of the kinetic-rate equation:

1. Triglycerides were the limiting reactant, whereas methanol was the excess reactant.
2. Triglyceride molecules were attached to the active sites and reacted with free-moving methanol molecules.
3. Glycerol was free-moving after transesterification, while FAME molecules remained attached to the vacant sites.
4. The surface reaction was assumed to be a rate-limiting step.

Given that the surface reaction was a rate-limiting step, $r_a = r_d = 0$; thus, Equations (4) and (7) were simplified as

$$C_{TG.S} = K_a C_{TG} C_S \quad (9)$$

$$C_{FAME.S} = \frac{C_{FAME} C_S}{K_d} \quad (10)$$

The vacant site of nano CaO catalyst could be derived by balancing the total active sites ($C_t$):

$$C_t = C_S + C_{TG.S} + C_{FAME.S} \quad (11)$$

$$C_t = C_S + K_a C_{TG} C_S + \frac{C_{FAME} C_S}{K_d} \quad (12)$$

$$C_t = C_S (1 + K_a C_{TG} + \frac{C_{FAME}}{K_d}) \quad (13)$$

$$C_S = \frac{C_t}{1 + K_a C_{TG} + \frac{C_{FAME}}{K_d}} \quad (14)$$

Equations (9), (10) and (14) were then substituted into Equation (5):

$$r_s = k_s C_{TG.S} C_M - k_{-s} C_{FAME.S} C_G \quad (15)$$

$$r_s = k_s K_a C_{TG} C_S C_M - k_{-s}\left(\frac{C_{FAME} C_S}{K_d}\right) C_G \quad (16)$$

$$r_s = \frac{C_t k_s K_a C_{TG} C_M}{1 + K_a C_{TG} + \frac{C_{FAME}}{K_d}} - k_{-s}\left[\frac{C_t C_{FAME}}{K_d\left(1 + K_a C_{TG} + \frac{C_{FAME}}{K_d}\right)}\right] C_G \quad (17)$$

Given that methanol was in excess, transesterification was assumed to be irreversible, and backward reaction could be ignored. As triglycerides were the limiting reactant, the low concentration produced $1 + K_a C_{TG} \approx 1$. FAME and glycerol detached from the active site in a rapid rate, and the ratio of $C_{FAME}$ to $K_d$ was approximately zero; thus, Equation (17) can be simplified to

$$r_s = kC_{TG} \quad (18)$$

where

$$k = C_t k_s K_a C_M$$

Given that $r_s = kC_{TG}$

$$-\frac{dC_{TG}}{dt} = kC_{TG} \quad (19)$$

with limit $C_{TG} = C_{TG0}$ at $t = 0$ gives

$$\ln \frac{C_{TG0}}{C_{TG}} = kt \quad (20)$$

Consequently, the plot slope of $\ln \frac{C_{TG0}}{C_{TG}}$ as a function of time was linear with slope $k$.

3.3.2. Kinetic Equation and Experiment Data

Figure 10 shows a series of experiment data that were obtained from the transesterification of palm oil catalyzed by nano CaO prepared via thermal hydration–dehydration treatment. The data were fit into the developed kinetic equation. The reaction rate was constant, and the $k$ value of the transesterification of palm oil catalyzed by nano CaO prepared via thermal hydration–dehydration treatment was 0.0007 $min^{-1}$ with an $R^2$ value of 0.9049. This shows that the kinetic mechanism—deduced on the basis of Langmuir–Hinshelwood kinetics that involve adsorption reaction, surface reaction, and desorption reaction—described well the catalytic mechanism of the nano CaO catalyst in converting triglycerides into biodiesel. Hence, the rate law that was developed on the basis of the kinetic mechanism could be used to model the transesterification reaction catalyzed by the nano CaO catalyst.

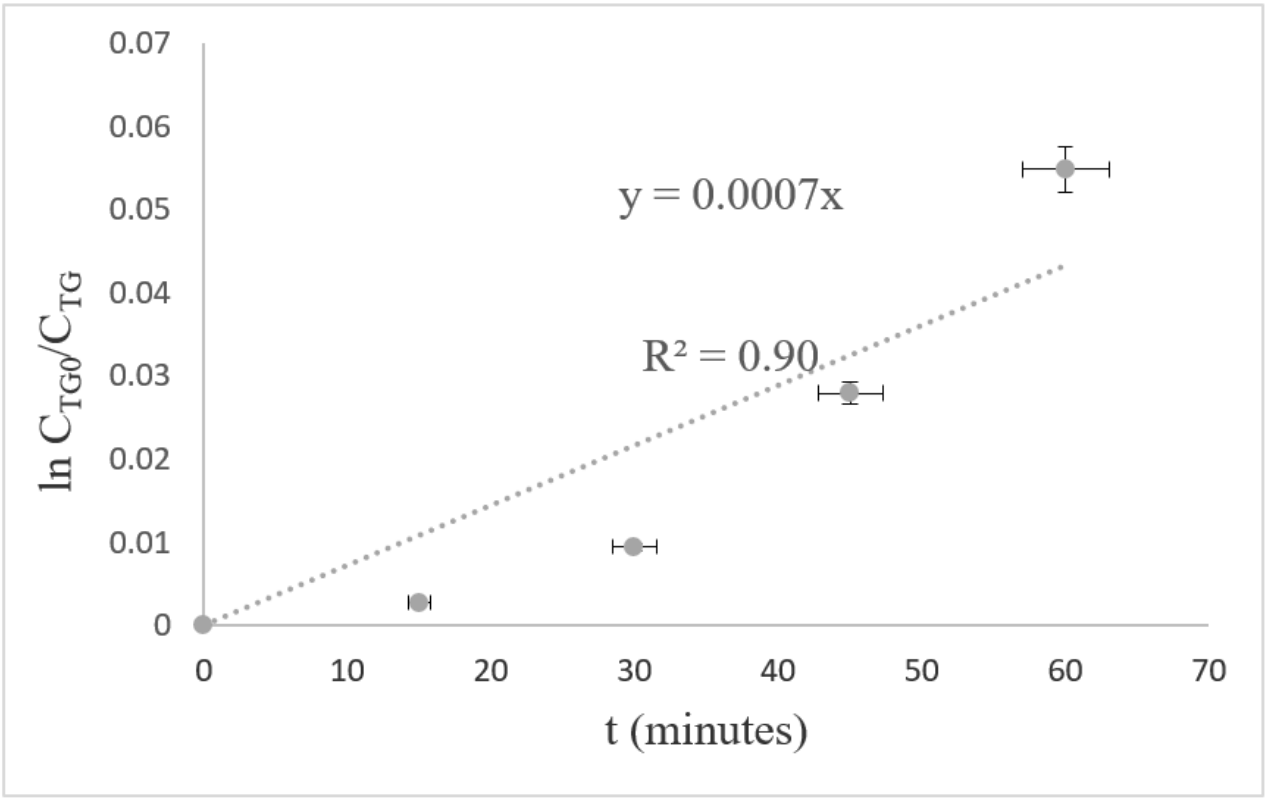



**Figure 10.** Plot of ln $\frac{C_{TG0}}{C_{TG}}$ versus time.

3.3.3. Activation Energy and Prefrequency Factor

In order to investigate the activation energy and pre-exponential constant of the transesterification reaction catalyzed by nano CaO, the Arrhenius equation was plotted. The derivation of the Arrhenius equation into a linear equation is shown below:

$$k = Ae^{\frac{-Ea}{RT}} \quad (21)$$

Taking the logarithmic form of Equation (21), the equation can be expressed as:

$$\ln k = \ln A - \frac{E_a}{RT} \quad (22)$$

where $k$ represents rate constants derived from the kinetic model, $A$ is the pre-exponential constant, $R$ is the universal gas constant (8.314 J/mol·K), $T$ is the absolute temperature in kelvin, and $Ea$ is the activation energy. Figure 11 shows the Arrhenius plot for transesterification reaction of palm oil at 45, 50, 55, and 60 °C.

Figure 11 shows that the activation energy and exponential constant calculated from the Arrhenius plot were 3786.69 J/mol and 1.677 $min^{-1}$, respectively. According to Freedman et al. [52], activation energy normally falls within the range of 33.6–84.0 kJ $mol^{-1}$ for base-catalyzed transesterification reactions. In the current study, the activation energy for the transesterification reaction of palm oil catalyzed by nano CaO was lower than the activation energy of base-catalyzed transesterification reactions. The nano CaO catalyst was successfully synthesized with the favorable catalytic properties of low activation energy that led to a high reaction rate and FAME yield.

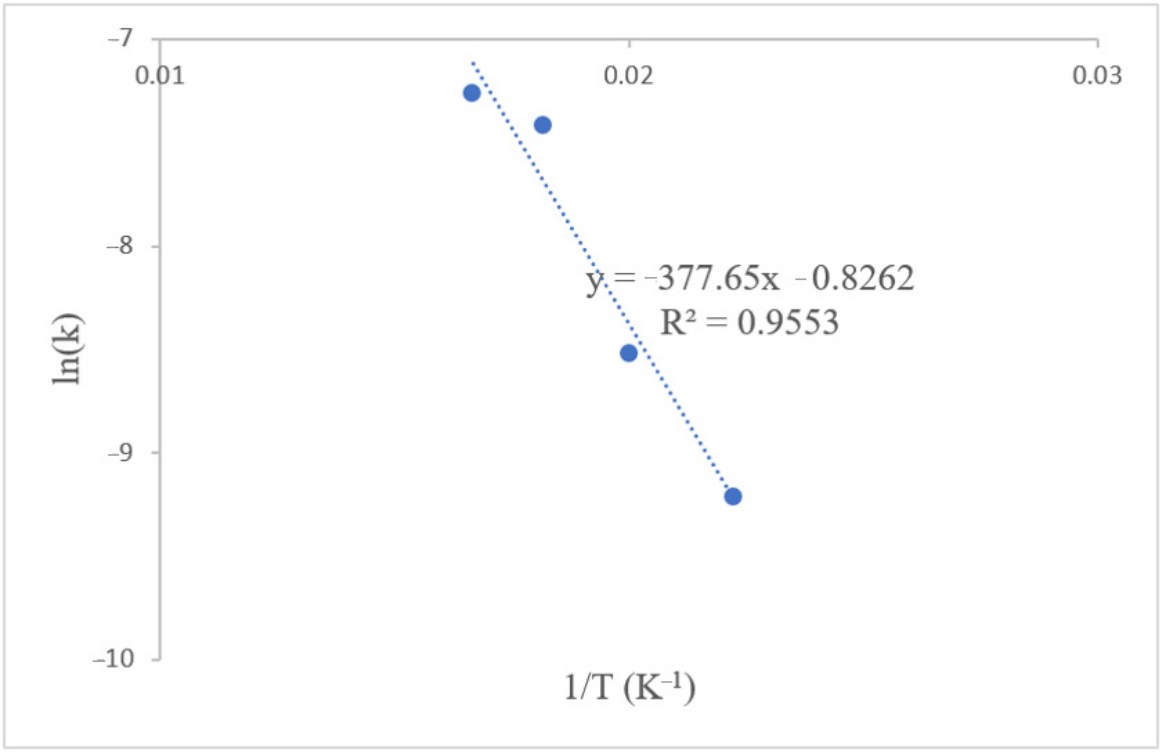



**Figure 11.** Arrhenius plot of transesterification reaction catalyzed by nano CaO catalyst.

## 4. Conclusions

A nano CaO catalyst with desired catalytic properties was successfully developed from waste cockle shells via thermal hydration–dehydration treatment. The optimal conditions for thermal hydration–dehydration treatment used to develop the nano CaO catalyst were 6 h of hydration duration, 650 °C of recalcination temperature, and 3 h of recalcination duration. Of biodiesel yield, 94.13% was obtained at a moderate temperature of 60 °C and 3 h reaction time during the transesterification of palm oil catalyzed by the nano CaO. The XRD diffraction pattern and elemental results confirmed the transformation of $CaCO_3$ in waste cockle shells to the nano CaO catalyst during thermal hydration–dehydration treatment. SEM, BET, and TPD results proved the CaO nanocatalyst with the existence of a large surface area (13.9113 $m^2/g$) and high pore volume (0.0318 $cm^3/g$) that were rich in vacant active sites (1046.46 μmol $CO_2/g$); the pore diameter (33.17 nm) was accessible to reactants (triglycerides, methanol) and products (FAME, glycerol). The kinetic mechanism with surface reaction as the rate-limiting step described well the transesterification reaction of palm oil catalyzed by the nano CaO catalyst. The utilization of the green nano CaO catalyst in the transesterification reactions significantly reduced activation energy to 3786.69 J/mol, thus accelerating the reaction rate to 27.3% FAME yield/h.

**Author Contributions:** Investigation, methodology, and writing—original draft, C.Y.C.; supervision, J.H.S., S.F.T. and Z.H.L. All authors have read and agreed to the published version of the manuscript.

**Funding:** This research was funded by the UTAR Research Fund (project no. IPSR/RMC/UTARRF/2018-C1/S01).

**Informed Consent Statement:** Not applicable.

**Acknowledgments:** The authors express their gratitude to the University Tunku Abdul Rahman (UTAR), Malaysia for the financial support in project funding through the UTAR Research Fund (project no. IPSR/RMC/UTARRF/2018-C1/S01).

**Conflicts of Interest:** The authors declare no conflict of interest. The funders had no role in the design of the study; in the collection, analyses, or interpretation of data; in the writing of the manuscript, or in the decision to publish the results.

## References

1. Looney, B. Statistical Review of World Energy, 2020 | 69th Edition. BP. 2020. Available online: https://www.bp.com/content/dam/bp/business-sites/en/global/corporate/pdfs/energy-economics/statistical-review/bp-stats-review-2020-full-report.pdf. (accessed on 3 February 2021).
2. Leung, D.Y.C.; Wu, X.; Leung, M.K.H. A review on biodiesel production using catalyzed transesterification. *Appl. Energy* **2010**, *87*, 1083–1095. [CrossRef]
3. Ahmad, A.L.; Yasin, N.H.M.; Derek, C.J.C.; Lim, J.K. Microalgae as a sustainable energy source for biodiesel production: A review. *Renew. Sustain. Energy Rev.* **2011**, *15*, 584–593. [CrossRef]
4. Borges, M.E.; Díaz, L. Recent developments on heterogeneous catalysts for biodiesel production by oil esterification and transesterification reactions: A review. *Renew. Sustain. Energy Rev.* **2012**, *16*, 2839–2849. [CrossRef]
5. Ezebor, F.; Khairuddean, M.; Abdullah, A.Z.; Boey, P.L. Oil palm trunk and sugarcane bagasse derived solid acid catalysts for rapid esterification of fatty acids and moisture-assisted transesterification of oils under pseudo-infinite methanol. *Bioresour. Technol.* **2014**, *157*, 254–262. [CrossRef]
6. Cheirsilp, B.; Louhasakul, Y. Industrial wastes as a promising renewable source for production of microbial lipid and direct transesterification of the lipid into biodiesel. *Bioresour. Technol.* **2013**, *142*, 329–337. [CrossRef]
7. Dehkhoda, A.M.; West, A.H.; Ellis, N. Biochar based solid acid catalyst for biodiesel production. *Appl. Catal. A Gen.* **2010**, *382*, 197–204. [CrossRef]
8. Balat, M. Production of biodiesel from vegetable oils: A survey. *Energy Sources Part A Recover. Util. Environ. Eff.* **2007**, *29*, 895–913. [CrossRef]
9. Talebian-Kiakalaieh, A.; Amin, N.A.S.; Mazaheri, H. A review on novel processes of biodiesel production from waste cooking oil. *Appl. Energy* **2013**, *104*, 683–710. [CrossRef]
10. Canakci, M.; Van Gerpen, J. Biodiesel production from oils and fats with high free fatty acids. *Trans. Am. Soc. Agric. Eng.* **2001**, *44*, 1429–1436. [CrossRef]
11. Karmakar, A.; Karmakar, S.; Mukherjee, S. Properties of various plants and animals feedstocks for biodiesel production. *Bioresour. Technol.* **2010**, *101*, 7201–7210. [CrossRef]
12. Borugadda, V.B.; Goud, V.V. Biodiesel production from renewable feedstocks: Status and opportunities. *Renew. Sustain. Energy Rev.* **2012**, *16*, 4763–4784. [CrossRef]
13. Kumar, N.; Varun; Chauhan, S.R. Performance and emission characteristics of biodiesel from different origins: A review. *Renew. Sustain. Energy Rev.* **2013**, *21*, 633–658. [CrossRef]
14. Yaakob, Z.; Mohammad, M.; Alherbawi, M.; Alam, Z.; Sopian, K. Overview of the production of biodiesel from Waste cooking oil. *Renew. Sustain. Energy Rev.* **2013**, *18*, 184–193. [CrossRef]
15. Atadashi, I.M.; Aroua, M.K.; Aziz, A.A. Biodiesel separation and purification: A review. *Renew. Energy* **2011**, *36*, 437–443. [CrossRef]
16. Sharma, Y.C.; Singh, B.; Korstad, J. Latest developments on application of heterogenous basic catalysts for an efficient and eco friendly synthesis of biodiesel: A review. *Fuel* **2011**, *90*, 1309–1324. [CrossRef]
17. Mosaddegh, E.; Hassankhani, A. Preparation and characterization of nano-CaO based on eggshell waste: Novel and green catalytic approach to highly efficient synthesis of pyrano[4,3-b]pyrans. *Chin. J. Catal.* **2014**, *35*, 351–356. [CrossRef]
18. Chen, G.-Y.; Shan, R.; Yan, B.-B.; Shi, J.-F.; Li, S.-Y.; Liu, C.-Y. Remarkably enhancing the biodiesel yield from palm oil upon abalone shell-derived CaO catalysts treated by ethanol. *Fuel Process. Technol.* **2016**, *143*, 110–117. [CrossRef]
19. Lesbani, A.; Okta, S.; Sitompul, C.; Mohadi, R.; Hidayati, N. Characterization and Utilization of Calcium Oxide (CaO) Thermally Decomposed from Fish Bones as a Catalyst in the Production of Biodiesel from Waste Cooking Oil. *Chem. Eng.* **2016**, *20*, 121–126. [CrossRef]
20. Reddy, C.; Reddy, V.; Oshel, R.; Verkade, J.G. Room-temperature conversion of soybean oil and poultry fat to biodiesel catalyzed by nanocrystalline calcium oxides. *Energy Fuels* **2006**, *20*, 1310–1314. [CrossRef]

21. Kesic, Z.; Lukic, I.; Zdujic, M.; Mojovic, L.; Skala, D. Calcium oxide based catalysts for biodiesel production: A review. *Chem. Ind. Chem. Eng. Q.* **2016**, *22*, 391–408. [CrossRef]
22. Islam, N.; Miyazaki, K. Nanotechnology systems of innovation: Investigation of scientific disciplines' fusion trend into nanotech. In Proceedings of the PICMET'07—2007 Portland International Conference on Management of Engineering & Technology, Portland, OR, USA, 5–9 August 2007; pp. 2922–2931.
23. Yilmaz, B.; Müller, U. Catalytic Applications of Zeolites in Chemical Industry. *Top. Catal.* **2009**, *52*, 888–895. [CrossRef]
24. Schmidt, F. New catalyst preparation technologies—Observed from an industrial viewpoint. *Appl. Catal. A Gen.* **2001**, *221*, 15–21. [CrossRef]
25. Zhang, Y.; Dubé, M.A.; McLean, D.D.; Kates, M. Biodiesel production from waste cooking oil: 1. Process design and technological assessment. *Bioresour. Technol.* **2003**, *89*, 1–16. [CrossRef]
26. Garrigue, P.; Delville, M.H.; Labrugère, C.; Cloutet, E.; Kulesza, P.J.; Morand, J.P.; Kuhn, A. Top-down approach for the preparation of colloidal carbon nanoparticles. *Chem. Mater.* **2004**, *16*, 2984–2986. [CrossRef]
27. Nadagouda, M.N.; Varma, R.S. Green and controlled synthesis of gold and platinum nanomaterials using vitamin B2: Density-assisted self-assembly of nanospheres, wires and rods. *Green Chem.* **2006**, *8*, 516–518. [CrossRef]
28. Kumar, D.; Ali, A. Nanocrystalline K–CaO for the transesterification of a variety of feedstocks: Structure, kinetics and catalytic properties. *Biomass Bioenergy* **2012**, *46*, 459–468. [CrossRef]
29. Zhao, L.; Qiu, Z.; Stagg-Williams, S.M. Transesterification of canola oil catalyzed by nanopowder calcium oxide. *Fuel Process. Technol.* **2013**, *114*, 154–162. [CrossRef]
30. Latchubugata, C.S.; Kondapaneni, R.V.; Patluri, K.K.; Virendra, U.; Vedantam, S. Kinetics and optimization studies using Response Surface Methodology in biodiesel production using heterogeneous catalyst. *Chem. Eng. Res. Des.* **2018**, *135*, 129–139. [CrossRef]
31. Ljupkovic, R.; Micic, R.; Tomic, M.; Radulovic, N.; Bojic, A.; Zarubica, A. Significance of the structural properties of CaO catalyst in the production of biodiesel: An effect on the reduction of greenhouse gases emission. *Hem. Ind.* **2014**, *68*, 399–412. [CrossRef]
32. Vujicic, D.; Comic, D.; Zarubica, A.; Micic, R.; Boskovic, G. Kinetics of biodiesel synthesis from sunflower oil over CaO heterogeneous catalyst. *Fuel* **2010**, *89*, 2054–2061. [CrossRef]
33. Micic, R.D.; Bosnjak Kiralj, M.S.; Panic, S.N.; Tomic, M.D.; Jovic, B.D.; Boskovic, G.C. Activation temperature imposed textural and surface synergism of CaO catalyst for sunflower oil transesterification. *Fuel* **2015**, *159*, 638–645. [CrossRef]
34. Chong, K.Y.; Chia, C.H.; Zakaria, S. Polymorphs calcium carbonate on temperature reaction. *AIP Conf. Proc.* **2014**, *1614*, 52–56.
35. Cho, Y.B.; Seo, G.; Chang, D.R. Transesterification of tributyrin with methanol over calcium oxide catalysts prepared from various precursors. *Fuel Process. Technol.* **2009**, *90*, 1252–1258. [CrossRef]
36. Roschat, W.; Phewphong, S.; Thangthong, A.; Moonsin, P. Catalytic performance enhancement of CaO by hydration-dehydration process for biodiesel production at room temperature. *Energy Convers. Manag.* **2018**, *165*, 1–7. [CrossRef]
37. Saoud, K.; Ibala, I.; Ladki, D.; Ezzeldeen, O.; Saeed, S. *Microwave Assisted Preparation of Calcium Hydroxide and Barium Hydroxide Nanoparticles and Their Application for Conservation of Cultural Heritage*; Springer: Cham, Switzerland, 2014.
38. Widayat, W.; Darmawan, T.; Hadiyanto, H.; Rosyid, R.A. Preparation of Heterogeneous CaO Catalysts for Biodiesel Production. *J. Phys. Conf. Ser.* **2017**, *877*, 012018. [CrossRef]
39. Tangboriboon, N.; Kunanuruksapong, R.; Srivat, A. Meso-porosity and phase transformation of bird eggshells via pyrolysis. *J. Ceram. Process. Res.* **2012**, *13*, 413–419.
40. Asikin-Mijan, N.; Taufiq-Yap, Y.H.; Lee, H.V. Synthesis of clamshell derived $Ca(OH)_2$ nano-particles via simple surfactant-hydration treatment. *Chem. Eng. J.* **2015**, *262*, 1043–1051. [CrossRef]
41. Putra, R.S.; Liyanita, A.; Arifah, N.; Puspitasari, E.; Sawaludin; Hizam, M.N. Enhanced Electro-Catalytic Process on the Synthesis of FAME Using CaO from Eggshell. *Energy Procedia* **2017**, *105*, 289–296. [CrossRef]
42. Yoosuk, B.; Udomsap, P.; Puttasawat, B.; Krasae, P. Modification of calcite by hydration–dehydration method for heterogeneous biodiesel production process: The effects of water on properties and activity. *Chem. Eng. J.* **2010**, *162*, 135–141. [CrossRef]
43. Smith, S.M.; Oopathum, C.; Weeramongkhonlert, V.; Smith, C.B.; Chaveanghong, S.; Ketwong, P.; Boonyuen, S. Transesterification of soybean oil using bovine bone waste as new catalyst. *Bioresour. Technol.* **2013**, *143*, 686–690. [CrossRef]
44. Galván-Ruiz, M.; Hernández, J.; Baños, L.; Noriega-Montes, J.; Rodríguez-García, M.E. Characterization of Calcium Carbonate, Calcium Oxide, and Calcium Hydroxide as Starting Point to the Improvement of Lime for Their Use in Construction. *J. Mater. Civ. Eng.* **2009**, *21*, 694–698. [CrossRef]
45. Menad, K.; Feddag, A.; Rubenis, K. Synthesis and study of calcination temperature influence on the change of structural properties of the LTA zeolite. *Rasayan J. Chem.* **2016**, *9*, 788–797.
46. Reli, M.; Kočí, K.; Matějka, V.; Kovář, P.; Obalová, L. Effect of calcination temperature and calcination time on the kaolinite/$TiO_2$ composite for photocatalytic reduction of $CO_2$. *Geosci. Eng.* **2012**, *58*, 10–22. [CrossRef]
47. Chang, H.J.; Crynes, B.L. Effect of Catalyst Pore and Pellet Sizes on Deactivation in SRC Oil Hydrotreatment. *AIChE J.* **1986**, *32*, 224–232. [CrossRef]
48. Shuit, S.H.; Ng, E.P.; Tan, S.H. A facile and acid-free approach towards the preparation of sulphonated multi-walled carbon nanotubes as a strong protonic acid catalyst for biodiesel production. *J. Taiwan Inst. Chem. Eng.* **2015**, *52*, 100–108. [CrossRef]
49. Ten Elshof, J.E.; Abadal, C.R.; Sekulić, J.; Chowdhury, S.R.; Blank, D.H.A. Transport mechanisms of water and organic solvents through microporous silica in the pervaporation of binary liquids. *Microporous Mesoporous Mater.* **2003**, *65*, 197–208. [CrossRef]

50. Jahn, D.A.; Wong, J.; Bachler, J.; Loerting, T.; Giovambattista, N. Glass polymorphism in glycerol-water mixtures: I. A computer simulation study. *Phys. Chem. Chem. Phys.* **2016**, *18*, 11042–11057. [CrossRef] [PubMed]
51. Yoosuk, B.; Udomsap, P.; Puttasawat, B. Hydration–dehydration technique for property and activity improvement of calcined natural dolomite in heterogeneous biodiesel production: Structural transformation aspect. *Appl. Catal. A Gen.* **2011**, *395*, 87–94. [CrossRef]
52. Freedman, B.; Butterfield, R.O.; Pryde, E.H. Transesterification kinetics of soybean oil 1. *J. Am. Oil Chem. Soc.* **1986**, *63*, 1375–1380. [CrossRef]